VPLIV VPADNEGA KOTA IN LASERSKEGA ODTISA NA NATANČNOST IN STOPNJO PODROBNOSTI PRI TERESTRIČNEM LASERSKEM SKENIRANJU

INFLUENCE OF INCIDENT ANGLE AND LASER FOOTPRINT ON PRECISION AND LEVEL OF DETAIL IN TERRESTRIAL LASER SCANNER MEASUREMENTS

Sajid Mahmood, Zulkepli bin Majid, Khairulnizam bin M. Idris, Muhammad Hamid Chaudhry

UDK: 528.71
Klasifikacija prispevka po COBISS.SI: 1.01
Prispelo: 9. 10. 2020
Sprejeto: 5. 6. 2021

DOI: 10.15292/geodetski-vestnik.2022.01.260-281
SCIENTIFIC ARTICLE
Received: 9. 10. 2020
Accepted: 5. 6. 2021

IZVLEČEK

Terestrični laserski skenerji (angl. terrestrial laser scanners *– TLS) se uporabljajo na različnih področjih, kot so geodezija, gozdarstvo, ohranjanje kulturne dediščine, rudarstvo, topografija, urbanistično planiranje, forenzika ipd. Navedena tehnologija je močno spremenila zbiranje prostorskih podatkov v 3D, predvsem z vidika hitrega zajema podatkov. Ni veliko priporočil glede georeferenciranja oblakov točk, zato se v praksi poskuša zajeti kar se da veliko elementov geometrije skeniranih objektov, predvsem zaradi bojazni, da bodo podatki skeniranja nepopolni. Pri načrtovanju skeniranja sta med drugim izrednega pomena zagotavljanje položajne točnosti in stopnje podrobnosti (angl. level of detail – LOD), ki sta odvisni od vpadnega kota, velikosti laserskega odtisa, prostorskega obsega in ločljivosti. V raziskavi smo razvili matematični model za različne konfiguracije površja skeniranja ob upoštevanju prostorskega obsega, vpadnega kota in odtisa laserskega žarka. Razviti model pomaga pri izbiri stojišča TLS za zajem podatkov z zahtevano položajno točnostjo in stopnjo podrobnosti. Modele smo verificirali z izpeljavo enega modela iz drugega s spreminjanjem vrednosti obravnavanih parametrov. Vplive vpadnega kota in velikosti odtisa laserskega žarka smo obravnavali matematično in eksperimentalno za primer naravne poševne površine. Na podlagi predstavljenih rezultatov lahko načrtujemo ustrezen položaj stojišča TLS, s katerim bomo dosegli zahtevano točnost in stopnjo podrobnosti.*

KLJUČNE BESEDE

terestrično lasersko skeniranje, vpadni kot, 3D izmera, digitalni model terena, oblak točk

ABSTRACT

Terrestrial laser scanners (TLS) are used for a variety of applications, e.g., surveying, forestry, cultural heritage preservation, mining, topographic mapping, urban planning, forensics etc. This technology has made a huge shift in 3D spatial data collection due to much faster speed compared to other techniques. In the absence of guiding principles for positioning TLS relative to an object, surveyors collect data at maximum arrangements of scanning geometry elements due to fear of incomplete data of TLS. In 3D spatial data acquisition, positional accuracy and Level of Detail (LOD) are major considerations and are dependent on laser incident angle, footprint size, range and resolution. Mathematical models have been developed relating range, incident angle and laser footprint size for different surface configurations. These models can be used to position TLS to collect data at required positional accuracy and LOD. Models have been verified by deriving one model from other surface models by changing parameters. Effects of incident angle and footprint size have been studied mathematically and experimentally on a natural sloping surface. From the results, surveyors can plan the positioning of the scanner so that data is collected at the required accuracy and LOD.

KEY WORDS

Terrestrial laser scanning, Incident Angle, 3D surveying, Digital Terrain Model, Point cloud

1 INTRODUCTION

Since 1990, when the world's first 3D commercial laser scanner was launched in the USA by Ben Kacyra, an Iraqi expatriate and civil engineer (Kościuk, 2012), this equipment is advancing technologically as well as its utility in diverse situations. Terrestrial Laser Scanner (TLS) or terrestrial LiDAR has created space in 3D data collection for a wide variety of applications (Kandrot, 2013) and has addressed the problems of data quality with no or minimal interference with other activities. In the last two decades, the technology of TLS is becoming popular amongst the surveying community because of its capability of collecting millions of 3D points within seconds with high accuracy. Most of the TLS systems are equipped with external or in-built cameras to acquire images of areas being scanned, thus capable of providing photorealistic 3D coloured point cloud (Luh *et al.*, 2014). To visualize the use of TLS in the multidisciplinary domain, it is enough to type the phrase "*Applications of Terrestrial Laser Scanner*" in google scholar, and one will find more than 51,000 search results, but if the search is made year-wise, the total results are even more than 85,000 till 2019 (Figure 1). It clearly indicates that TLS is now a well-recognized, trusted and well-established technology for direct 3D measurements.

Russhakim *et al.* (2019) compared TLS with Mobile Laser Scanning during a building survey and mapping application and found better accuracy results for TLS. Its data can be integrated with other sensors like ALS for better reconstruction of 3D objects like building reconstruction, as done by Abdullah *et al.*(2017). An overview of the use of this technology for different projects, including the accuracy achieved, efficiency and analysis, can be found in Pinkerton (2011). A detailed review of this technology, its geometric and radiometric characteristics can be found in Mahmood *et al.* (2018).

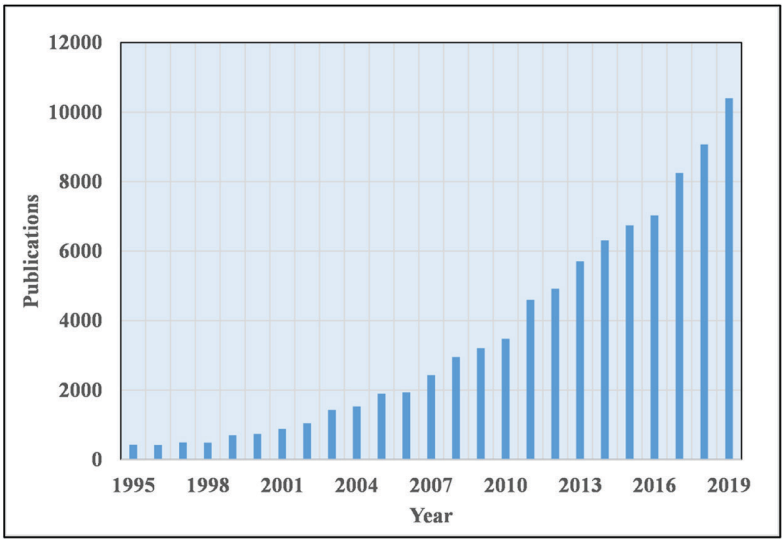

Figure 1: Google scholar search results in line with (Cheng *et al.*, 2018) on "Applications of Terrestrial Laser Scanners" phrase (Accessed on June 13, 2020).

The accuracy of 3D point cloud depends upon the type of scanner, i.e. Time of Flight (ToF) or phase-based, mechanical assembly precision, e.g. rotation mechanism, geometrical aspects/parameters of scanning, e.g. range, incident angle, laser footprint, feature surface properties, environmental impacts, mixed

pixel phenomenon, thermal expansion, instrument vibration and errors in post-processing of point cloud due to registration and filtering processes (Soudarissanane *et al.*, 2008; Reshetyuk, 2009; Lichti, 2010a). Out of the above geometrical properties, incident angle, laser footprint, and range are directly related to each other and affects the accuracy and Level of Detail (LoD - what minimum size of an object is to be mapped) of the scanned object/area. So to effectively use this technology for 3D surveying, mathematical models have been developed for both parameters of incident angle and laser footprint for the study of their variation with range. These models can further be used for modelling of inaccuracies induced due to these parameters. After development of models, this paper focused on experimental study for their effects on Digital Terrain Model (DTM). The effect on LoD will be dealt in future. The developed models and results of this study can be used for positioning TLS for optimal results both in accuracy and LoD.

2 RELATED STUDIES

The incident angle is the angle between the incident laser beam and the surface normal in the case of plane surface (Figure 2), and in the case of a curved surface, it is the angle between the incident laser beam and normal to the tangent plane at the point of incidence. Since the normal is defined as a vector pointing outwards and perpendicular to the plane surface or tangent plane so it will always remain in the interval $[0^0 \leq \alpha \leq 90^0]$.

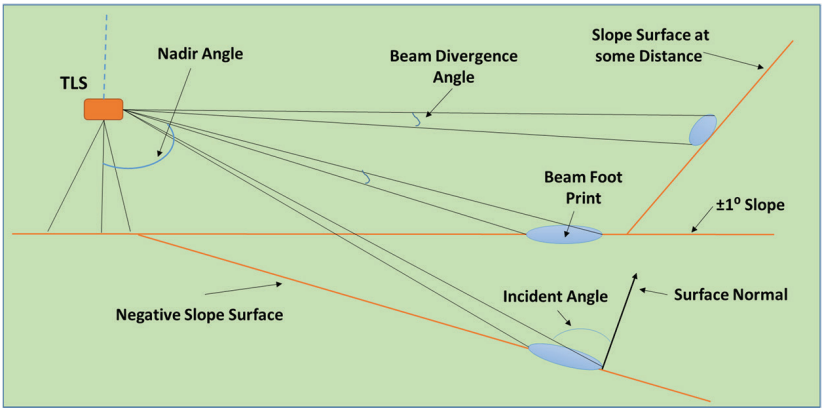

Figure 2: Incident angle schematic representation.

The incident angle affects the reflected energy. Power distribution across the pulse is not uniform but can be considered as symmetrical Gaussian distribution with maximum energy concentrated within the footprint (Schaer *et al.*, 2007). The laser beam shape, spot size and reflectivity from the target are dependent on the incident angle. The backscattered signal from the target surface will be a function of the integrated energy distribution across the whole footprint. Theoretically, as per radar range Equation (1), the reflected intensity of TLS is directly proportional to the cosine of incidence angle (Tan and Cheng, 2016).

$$P_r = \frac{P_t D_r^2 \rho \cos\alpha}{4R^2} \eta_{sys} \eta_{atm} \tag{1}$$

where P_r is received laser power, P_t is transmitted laser power, D_r is receiver aperture diameter, R is Range, ρ is scanned target reflectance, α is incident angle and η_{sys} and η_{atm} are system transmission and atmos-

pheric transmission factors. This proportionality means that at larger incident angles, less reflectivity and hence adverse effects on accuracy. This is because laser spot deformed to an elliptical shape compared to the orthogonal alignment of beam, resulting in less reflectivity, affecting the scanned distance and, hence, 3D accuracy. It can be explained in two ways; firstly, the ellipse centre deviates from the point to which the distance is being measured, thus elongating the distance; secondly, more signal strength is reflected from the closer part of the elliptical spot leading to shortening of distance. Kersten *et al.* (2008) tested five different scanners for investigation of effects of incident angle and found that an increase in angle results in a decrease in geometric accuracy of objects, and also ToF scanners are influenced less than the phase difference scanners. They have not modelled the effect but just measured the effect of incident angle for different scanners. Soudarissanane et al. (2008) observed that density, intensity and accuracy of point cloud decrease with an increase in incident angle. They used phased based scanner, and measurements were made from a distance of 10 m only. Kersten *et al.* (2009) stated that the accuracy of any laser scanner is adversely influenced by incident angles of more than 45o and again reported that ToF scanners are less affected as compared to phase difference scanners. Soudarissanane *et al.* (2009) and Soudarissanane *et al.* (2011) developed a mathematical model of the influence of incident angle on range. The test of the model revealed that incident angle contributes approximately 20 % to the total error budget of a particular scan point. Voegtle and Wakaluk (2009) observed a decrease of about 0.4 mm in the standard deviation of range measurement with an increase in incident angle. They attributed this phenomenon towards that particular laser scanner (HDS 6000, Leica) used for the scanning by saying that it might be due to its characteristics of higher accuracy for angle as compared to range. Zámečníková *et al.* (2015) investigated and quantified the effect of incident angle using a TOF scanner and total station on reflectorless distance measurement from different distances ranging from 3.5 m to 30 m. They observed that effect of incident angle is not as prominent as of other factors at close ranges of 3.5 and 5.2 m but detected a systematic effect of 1.7 mm and 2.0 mm for rough and smooth surface respectively at 30 m range.

Lichti *et al.* (2005a) modelled the effect of laser beam width as an uncertainty in the horizontal and vertical angles which affects the range and quantifies an approximate range error of 0.15 m for a 3 mrad beam divergence and 45º incident angle at 100 m range for a Cyra Cyrax 2500 laser scanner. Lichti *et al.* (2005b) conducted an experiment to calculate the systematic bias because of laser beam width by scanning eight times a 4.5×3.3×80 m corridor using Riegl LMS-Z210 scanner (3 mrad divergence, i.e. 150 mm diameter at 50 m) and compared these measurements with the total station. They observed systematic beam width error but were unable to predict the value because the error in their scan setup was not only due to beam width but was strongly correlated with incident angle, however they recommended that beam width error must be considered in ground surveys for scanners having broad beam width. Soudarissanane (2016) rearranged the equations developed by (Sheng, 2008) to model laser beam footprint size for different surface configurations and used those for modelling of TLS laser beam footprint size. These equations for TLS are only applicable for vertical planes at some distance from TLS.

The laser footprint, which depends on range, incident angle and beam divergence, will affect the resolution of the scan and hence LoD because the final spot size illuminates certain area on striking the target. The average of attributes within the spot area is recorded by the receiver. Thus due to the larger spot size diameter, the survey result will have less overall detail on objects smaller than spot size. Also, if two lasers are hitting the same target at the same distance, the one that has a small spot size due to smaller beam

divergence will result in increased resolution and finer details. The other will produces low resolution due to larger divergence and spot size and hence fewer details (Bruce et al., 2016).

From the above discussion, it can be deduced that the effect of incidence angle on quality of point cloud has no acceptable model or value which can be applied during scanning for the topographic survey. And as per Kaasalainen *et al*. (2011), the possible correction for incidence angle effects on intensity which affects 3D accuracy, should also include information on the target surface reflectivity, which is not possible for the topographic survey. In the absence of this, a surveyor is unable to apply corrections for incident angle if at all significant or otherwise to point cloud. This necessitates investigation for optimal incident angle and spot size considering the effects of beam divergence and range for the topographic survey.

3 METHODOLOGY

In survey design, it is the first step to define the position of TLS so that maximum coverage and LoD at required accuracy could be achieved. Accuracy, along with other factors, is also affected by the angle of incidence and laser beam footprint size. Mathematical models have been developed to evaluate the variation of incidence angle and laser beam footprint size with range for different surface configurations, as shown in Figure 2. The mathematical correctness of these models has been checked by deriving a model for one surface configuration from the model of another surface configuration. From these mathematical modelling, graphs were plotted for observing the variation of incident angle, and laser beam footprint size with range and conclusions were drawn. The efficacy of the developed models based on conclusions has been elaborated in section 6. This was followed by the investigation of the effects of incident angle and beam footprint on DTM through field experimentation. The layout of the field experimentation is depicted in Figures 14 and 15. To see the effect on DTM, firstly, a base DTM was generated from the TLS position having the least values of incident angle and laser beam footprint size. Subsequently, six more DTMs were generated from different TLS positions by increasing the values of incident angle and laser beam footprint size. These DTMs were subtracted from the base DTM to see the difference, which actually is impacted by the incident angle and laser beam footprint size.

4 INCIDENT ANGLE MODELLING AND ITS EFFECTS

The scanner measures the backscattered reflected energy, which generally retraces the incident beam path. The amount or intensity of reflected light depends on the surface properties and the scanning geometry. A laser beam with zero incident angle, i.e. hitting the object perpendicularly, will have a circular footprint, whereas all other hits will result in elliptical-shaped footprints on the surface. Energy distribution will be the same along all radial sections in case of a zero-incident angle compared to the elliptical footprint. At the same range, the reflected energy is more in the case of zero-incident angle as compared to non-zero hits. It means that reflected intensity will keep decreasing with an increase in incident angle.

A lower intensity of the reflected signal means a deteriorated Signal to Noise Ratio (SNR). Since the detection unit of TLS generally uses a threshold value to distinguish between noise and the reflected signal so, if a signal is too weak, it will not be detected as a reflected signal. A signal is weak when its magnitude is smaller than the noise level of the detection unit. For longer distances or higher incident angles, the detection of the signal becomes harder, and some signals are even rejected, having less energy than the noise level.

4.1 Incident Angle Variation for Horizontal Surfaces

For horizontal surfaces, only the vertical angular increment capability of the instrument affects the incident angle, whereas horizontal angular increment traces a circular path, so no change in the range of laser beam. Figure 3 illustrates the concept of incident angle in the case of horizontal surface. 'E' is the TLS located at 'F' having instrument height 'h'. 'R' is the range of incident laser beam hitting at point 'A' making angle 'θ' with the nadir. 'α' and 'N' are the incident angle and corresponding normal vector respectively to the surface.

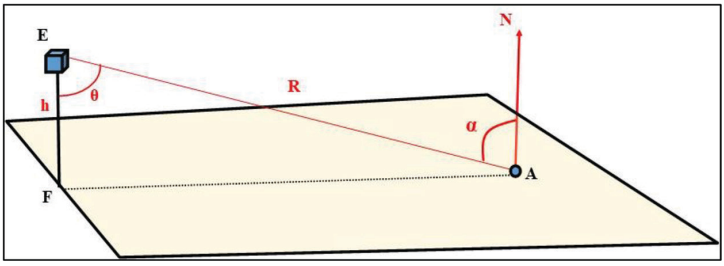

Figure 3: Incident angle for the horizontal surface.

By sine law in ΔAEF,

$$\frac{R}{\sin 90°} = \frac{h}{\sin(90° - \alpha)} \rightarrow \qquad \alpha = \cos^{-1}\left(\frac{h}{R}\right) \tag{2}$$

Equation (2) illustrates that as the range increases, the incident angle also increases. This increase is shown in Figure 4.

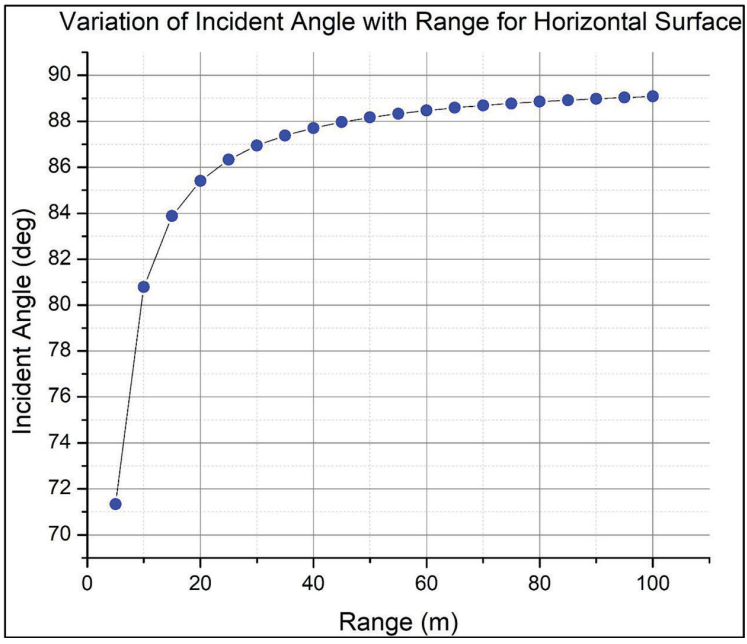

Figure 4: Incident angle variation with range for the horizontal surface.

The graph of Figure 4 has been drawn for an instrument height of 1.6 m. It can be seen from the graph that the incident angle reaches 85⁰ at a range of just 20 m and then approach asymptotically to 90⁰. If a topographic survey is planned based on previous literature which generally recommends scanning below 45⁰ (Daliga and Kurałowicz, 2016), below 55⁰ (Zámečníková *et al.*, 2015) and below 65⁰ (Lichti, 2007, Soudarissanane *et al.*, 2009) of incident angle, then it can be seen from the graph that useful range is less than 5 m which renders TLS totally inefficient whereas it has been observed by authors that a compatible quality DTM can be generated even beyond a range of 100 m and up to 200 m for horizontal surface.

4.2 Incident Angle Variation for Sloping Surfaces

Consider Figure 5, which represents a surface making an angle of 'γ' with the horizontal and scanner is placed at the foot of sloping surface. All other notations are as explained above in Figure 3.

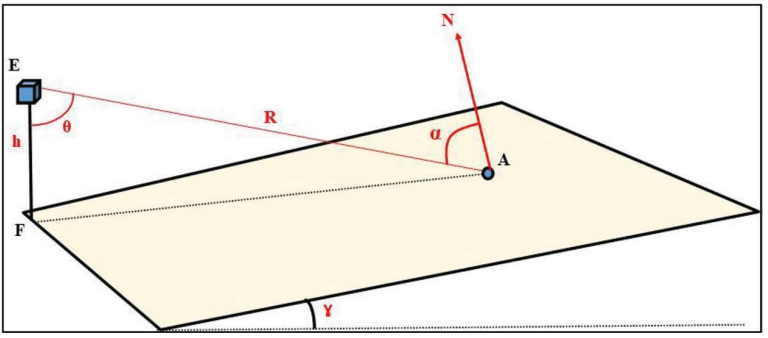

Figure 5: Incident angle for the positive sloping surface. Modified from (Mahmood et al., 2020).

By sine law in ΔAEF

$$\frac{R}{\sin(90°-\gamma)} = \frac{h}{\sin(90°-\alpha)} \quad \rightarrow \quad \frac{R}{\cos\gamma} = \frac{h}{\cos\alpha} \tag{3}$$

Therefore the incident angle at laser point 'A' is given by,

$$\alpha = \cos^{-1}\left(\frac{h}{R}\cos\gamma\right) \tag{4}$$

Equation (4) renders the same incident angle as obtained from Equation (2) for horizontal surface by substituting γ = 0⁰. The graphs of Equation (4) for γ = 5⁰ and γ = 45⁰ are shown in Figure 6.

The graphs of Figure 6 depicts the same behaviour of change in incident angle as depicted in the case of horizontal surface in Figure 4. The only difference is that as the slope of the surface increases, so as the incident angle for the same range. This can be seen for the initial three values of incident angles for γ = 0⁰, γ = 25⁰ and γ = 45⁰ which are approximately 71⁰, 73° and 77⁰ for a range of 5 m. This information leads to the conclusion that the scanner should not be placed within 5 m of the foot of any sloping surface. The same graphs are the output in case of a negative sloping surface, as shown in Figure 7. The reason for the same graphs is the same final equation for incident angle as Equation (4) because sine of the angle at point 'F' renders the same value, i.e. Sin (90⁰ - γ) = Sin (90⁰ + γ) = cosγ.

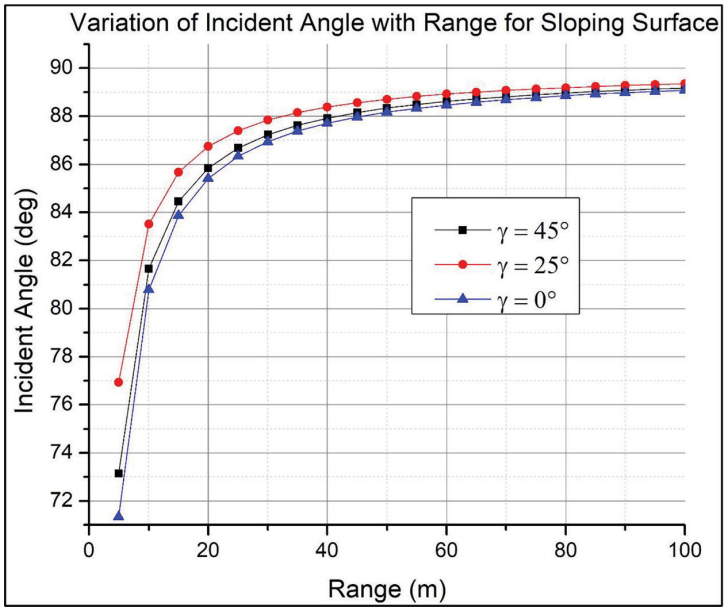

Figure 6: Incident angle variation with range for the sloping surface.

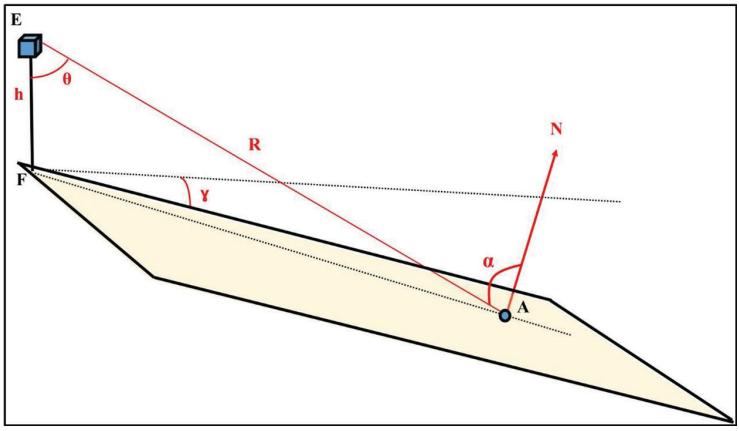

Figure 7: Incident angle for the negative sloping surface. Modified from (Mahmood et al., 2020).

4.3 Incident Angle Variation for Sloping Surface at Some Distance from Scanner

This surface is depicted in Figure 8, and all parameters are the same as explained in previous sections except 'd', which is the shortest distance to a surface perpendicular to the line 'BC' and instrument height 'EF' and 'φ' is the angle in the horizontal plane. In ΔEBC,

$$EC = \frac{d}{\cos\varphi} \tag{5}$$

In ΔAEC, by sine law in terms of 'α';

$$\frac{\frac{d}{\cos\varphi}}{\sin(90^0-\alpha)}=\frac{R}{\sin(180^0-\gamma)} \quad \rightarrow \quad \alpha=\cos^{-1}\left(\frac{d\sin\gamma}{R\cos\varphi}\right) \tag{6}$$

which is the incident angle 'α';

and in terms of 'θ', range 'R' can be expressed as

$$\frac{EC}{\sin\{90°+(\gamma-\theta)\}}=\frac{R}{\sin(180°-\gamma)} \quad \rightarrow \quad R=\frac{d\sin\gamma}{\cos\varphi\cos(\gamma-\theta)} \tag{7}$$

For γ = 90°, φ = 0° and θ = 90°, Equation (7) renders R = d and subsequently from Equation (6) α = 0°, which confirms the model.

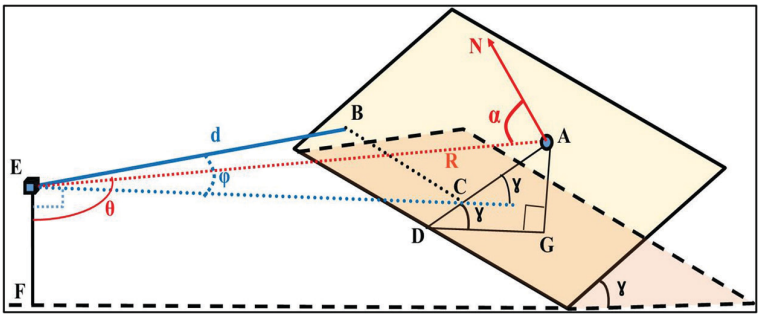

Figure 8: Incident angle for the sloping surface at some distance = d from the scanner. Modified from (Mahmood *et al.*, 2020).

Using values of 'd' and 'γ' as 20 m and 50⁰ respectively and for different values of 'θ' and 'φ', corresponding values of 'R' and incident angle 'α' calculated from Equations (7) and (6) respectively are as shown in Table 1.

Table 1: A Sample of calculations for incident angle and corresponding parameters.

d (m)	γ (deg)	θ (deg)	φ (deg)	R (m)	α (deg)
20	50	90	0.0	20.0	40.0
20	50	99	9.0	23.6	49.0
20	50	111	21.0	33.9	61.0
20	50	117	27.0	44.0	67.0
20	50	129	39.0	103.3	79.0
20	50	135	45.0	248.6	85.0

The variation of incident angles with range for two values of 'γ' has been plotted and is shown in Figure 9.

The following can be observed from Table 1 and the graphs of Figure 9:

- The behaviour of change of incident angle for the sloping surface at a distance 'd' from the scanner (Figure 8) is the same as in the case of horizontal and sloping surfaces above (Figures 5 and 7), i.e. it approaches asymptotically to 90⁰.
- With an increase in surface slope, incident angle decreases, and so the scanner should be placed optimally away from the surface, keeping in view other geometrical parameters.

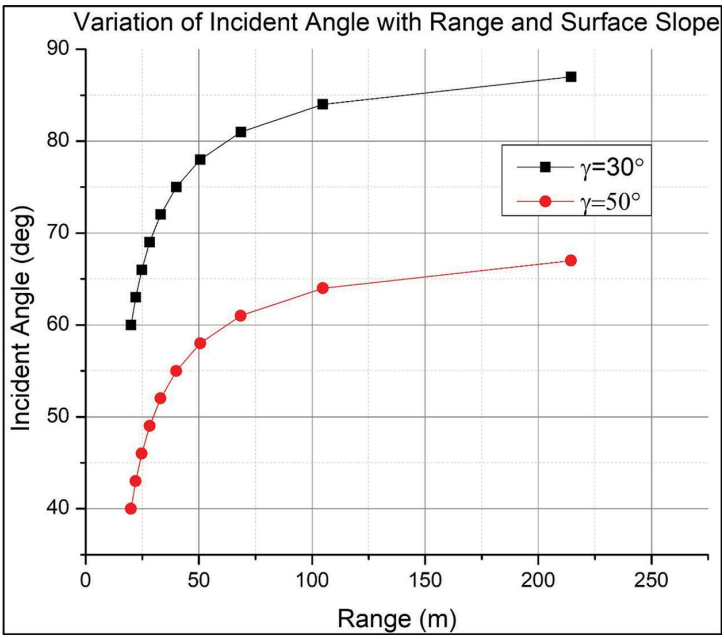

Figure 9: Incident angle variation for the sloping surface at a distance, d = 20 m from the scanner.

5 BEAM FOOT PRINT MODELLING AND ITS EFFECTS

Laser beam width is considered one of the intrinsic properties of the scanner, affecting positional uncertainty and spatial resolution. As explained above that the apparent location of the range observation is along the centerline of the emitted beam, but the actual point location cannot be predicted since it could lie anywhere within the projected beam footprint.

5.1 Beam Foot Print Size on Horizontal Surface

Assuming range observation along the centreline of the beam, its footprint size can be modelled as in Figure 10.

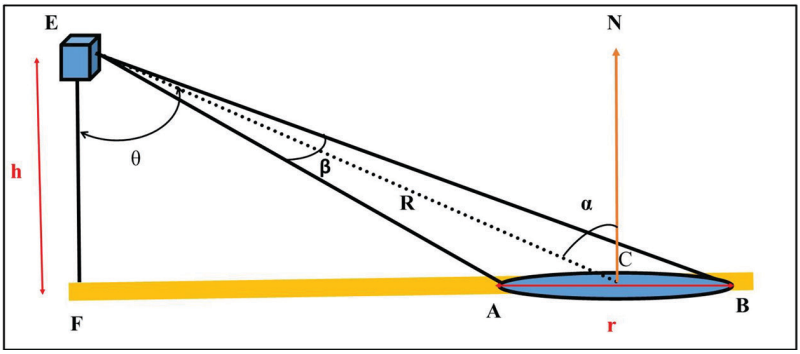

Figure 10: Schematic layout of TLS beam footprint for the horizontal surface.

The footprint of the laser beam away from TLS will be like an ellipse, as shown in Figure 10. The major axis being the most critical will be modelled here. Let 'β' denotes the beam divergence, 'r' as the major axis of elliptical footprint and rest terminologies are as already explained in previous sections. In this case, the angle 'α' is the same as the scanning angle 'θ'.

By sine law in ΔAEC,

$$AC = \frac{R \sin \frac{\beta}{2}}{\cos\left(\theta - \frac{\beta}{2}\right)} \tag{8}$$

Similarly, in ΔBEC:

$$CB = \frac{R \sin \frac{\beta}{2}}{\cos\left(\theta + \frac{\beta}{2}\right)} \tag{9}$$

Therefore, the length of the major axis will be AB = AC + CB, which after trigonometric simplifications, becomes;

$$AB = r = \frac{R \cos\theta \sin\beta}{cos^2 \frac{\beta}{2} - sin^2\theta} \tag{10}$$

Which in terms of instrument height 'h' can be written as:

$$r = \frac{\mathrm{h} \sin\beta}{cos^2 \frac{\beta}{2} - sin^2\theta} \quad where \quad h = R\cos\theta \tag{11}$$

For h = 1.6 m, θ = 85°, β = 7.33335E-05 radians, the values of 'R' and 'r' can be calculated using Equation (11) as 18.4 m and 15.5 mm respectively.

The variation of major axis length 'r' is plotted against the range 'R' for instrument height of 1.6 m and beam divergence of β = 0.0042017° (Topcon, 2019), is as depicted in Figure 11.

From Figure 11, it can be seen that at a range of 100 m, the length of the major axis of the elliptical footprint of the laser beam is approximately 475 mm. Since for horizontal surface, there is no significant change in the height of ground points, and also there is no question of detection of any small object during DTM creation, so there is no effect of footprint size in final DTM which means that a range of 100 m or more for the horizontal surface is acceptable for DTM generation. But for the detection of objects, the size of the major axis has to be less than or equal to half of the object size. Similarly, the beam footprint can be modelled for sloping surface using the terminologies used in Figures 5 and 6.

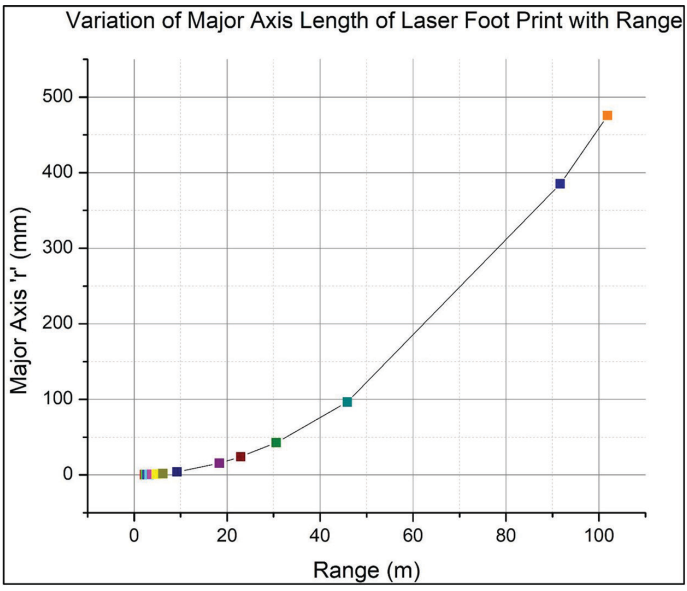

Figure 11: Variation of major axis length of elliptical footprint with range for the horizontal surface.

5.2 Beam Foot Print Size on Vertical and Inclined Surfaces

The elliptical footprint size 'AB' of the laser beam on an inclined surface at any distance 'd' from the scanner can be modelled using the visualized schematic diagram shown in Figure 12.

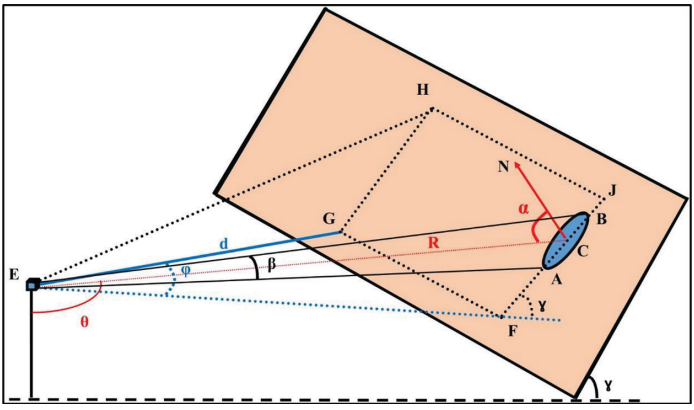

Figure 12: Schematic layout of laser beam footprint on an inclined surface. Modified from (Mahmood *et al.*, 2020).

All terminologies have already been explained in previous sections. Different angles in different triangles and subsequent steps are as explained below. By sine law in ΔAEC and ΔBEC:

$$\frac{AC}{\sin\frac{\beta}{2}} = \frac{R}{\sin\left\{90° + (\theta - \gamma - \frac{\beta}{2})\right\}} \rightarrow AC = \frac{R\sin\frac{\beta}{2}}{\cos(\theta - \gamma - \frac{\beta}{2})} \tag{12}$$

$$\frac{CB}{\sin\frac{\beta}{2}} = \frac{R}{\sin\left\{90° - (\theta - \gamma + \frac{\beta}{2})\right\}} \rightarrow CB = \frac{R\sin\frac{\beta}{2}}{\cos(\theta - \gamma + \frac{\beta}{2})} \tag{13}$$

$$\text{Hence AB} = \text{AC} + \text{CB} \rightarrow AB = \frac{R\sin\frac{\beta}{2}}{\cos(\theta - \gamma - \frac{\beta}{2})} + \frac{R\sin\frac{\beta}{2}}{\cos(\theta - \gamma + \frac{\beta}{2})} \tag{14}$$

$$AB = \left[\frac{R\cos(\theta - \gamma)\sin\beta}{\cos^2\frac{\beta}{2} - sin^2(\theta - \gamma)}\right] \tag{15}$$

where 'R' can be calculated from ΔEFC using sine law as:

$$\text{'R' can be calculated from } \Delta\text{EFC using sine law as} \rightarrow R = \frac{d\sin\gamma}{\cos\varphi\cos(\theta - \gamma)} \tag{16}$$

Equations (15) and (16) can be used for vertical surface by substituting $\gamma = 90^0$ and reduces to:

$$AB = \left[\frac{R\sin\theta\sin\beta}{\cos^2\frac{\beta}{2} - cos^2\theta}\right] \quad and \quad R = \frac{d}{\cos\varphi\sin\theta} \tag{17}$$

As a confirmatory check on the authenticity of Equations (15) to (17), for vertical surface at incident angle of 0^0 i.e. when $\theta = 90^0$, $\gamma = 90^0$, and $\varphi = 0^0$, these equations becomes;

$$AB = \left[\frac{R\sin\beta}{\cos^2\frac{\beta}{2}}\right] \quad and \quad R = d \tag{18}$$

$$\text{After simplification} \quad AB = \frac{d^*2\sin\frac{\beta}{2}\cos\frac{\beta}{2}}{\cos^2\frac{\beta}{2}} \rightarrow AB = 2d\tan\frac{\beta}{2} \tag{19}$$

Equation (19) confirms the correctness of Equations (15) to (17) for footprint size. Also, as per the specifications of Topcon TLS model GLS 2000 (Topcon, 2019), the spot size is less than or equal to 11 mm at a range of 150 m. By substituting the values of $\varphi = 0^0$, $\theta = 90^0$, $\gamma = 90^0$, $\beta = 0.0042017^0$ and d = 150 m in Equations (15) and (16), the value of 'AB' comes out is 11 mm, which further confirms the validity of the model. It should be noted that only the major axis has been modelled being more in length, and if at some value of it, its effect on data is acceptable, then the minor axis will definitely be acceptable, being shorter in length.

The plots of range versus footprint major axis from Equations (17) for the vertical surface at d = 30 m with parameters representing lines GH and GF of Figure 13 are the same and is shown in Figure 13a, whereas the graph for the same quantities with parameters representing line GJ is shown in Figure 13b.

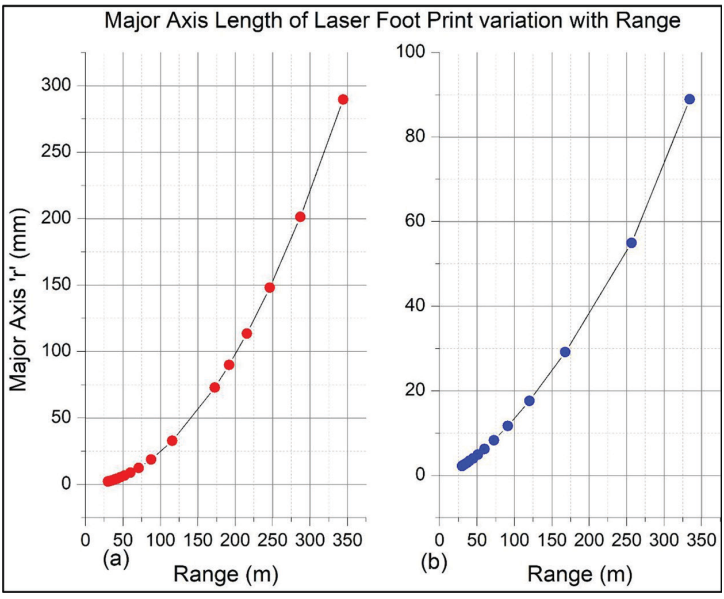

Figure 13: Variation of laser beam footprint major axis length with range for vertical surface for d = 30 m (a) along lines GH and GF (b) along line GJ of Figure 12.

For vertical surface at a distance d = 30 m from the scanner, the maximum length of the major axis of beam footprint is approximately 290 mm at a range near 350 m. But this depends on the distance 'd' of the scanner from the vertical surface. It is also seen from Figures 11 and 13 that the variation behaviour of footprint size with range is the same for horizontal and vertical surfaces except for the difference in corresponding values. With the models, it is possible to calculate footprint size for any configuration of parameters related to the surface depicted in Figure 12.

6 EFFICACY OF MODELS

For identification of any object in FoV, the distance between adjacent laser beam footprints must be less than or equal to half of the dimension of an object. It should also be noted that in laser scans, object identification also depends on the size of the beam footprint. If the footprint size is larger than the object dimension, the object will not be identifiable or could not be mapped. Thus for any object to be identifiable in the scan, the two criteria must be fulfilled, firstly the interspacing of adjacent points should be smaller than object size, and secondly, the footprint size should also be smaller than the object dimension. As an example, during the scanning of the façade of a building, as shown in Figure 14, the surveyor can adjust the location of the scanner for the LOD required.

If it is required to map/locate the railings present on the building façade marked in a red circle whose blow up is depicted on the right side of Figure 14, a surveyor needs to measure the parameters 'd', 'φ', 'θ' and 'R' and then can use relevant equations as in this case, equation 17 to calculate the laser footprint size. By comparing the size of footprint and railing size, the surveyor can decide whether the railing will be mapped or not and then readjust the scanner location. It should be noted that for mapping any object, the footprint should be less than the dimension of the object. Thus the models proposed could be used

beforehand to calculate the footprint size and then relocate the scanner if necessary. This paper aims to study the effect of incident angle and footprint size on precision in 3D surveying, so it will be studied in the next paragraphs, and object identification using these models will follow in future.

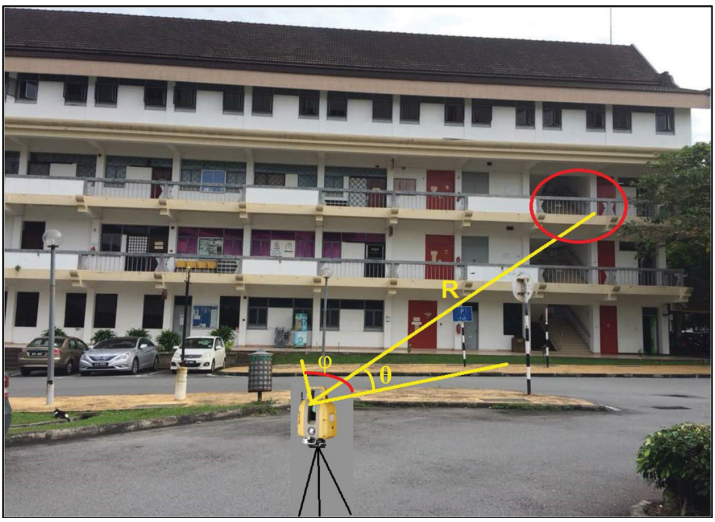

Figure 14: Planning for Locating a TLS for Surveying Required LOD. Adapted from (Mahmood et al., 2020).

7 PRACTICAL REALIZATION OF INCIDENT ANGLE AND FOOTPRINT SIZE

Investigating the effects of incident angle and laser footprint size on point cloud product, i.e. the DTM through practical experimentation, is explained in the following paragraphs.

7.1 Experimental Setup

In contrast to typical laboratory tests, it was intended to investigate the effects of incident angle on the point cloud on the natural landscape, which is the main focus of this study, i.e. topographic surveying. The biggest challenge was to design the test in the natural environment in such a way so that errors from other sources should either be avoided or annulled during processing, and only effects of incident angle could be studied. The main sources of errors in focus were due to range and registration/georeferencing processes. The test site intended was a vertical wall or nearly vertical slope having a minimum of 100 m clear field of view so as to find incident angle effects with more than 95 % confidence level from a minimum of two different ranges. This type of natural slopes or walls were available but were devoid of the intended field of view for scanning. The only site available was a small portion of the side slope of football ground having a 50 m of the field of view, as shown in Figure 15.

The portion of slope selected for the test is about 10 m x 20 m in size as marked in Figure 15(b), having a slope of approximately 26^0. The site was thoroughly cleaned of any debris, and also the grass was cut to almost zero levels so as to avoid any errors resulting from these in DTM. For marking the locations of scanning and prism stations, a small nail in a wooden wedge was used, as shown in Figure 15(c) to minimize the error due to location displacement. The scanning setup consists of the scanning site marked with a black rectangle and seven scanning stations marked with numbers from 1 to 7 in Figure 16.

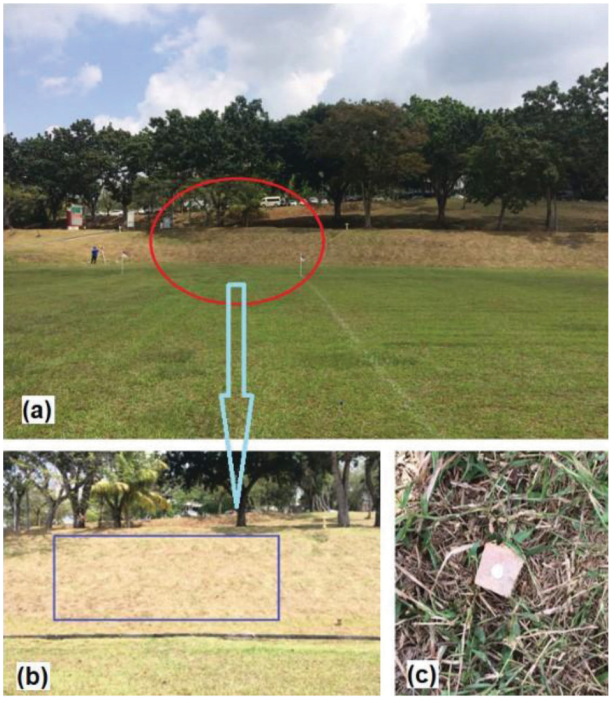

Figure 15: Test site for incident angle effects inside UTM, Skudai.

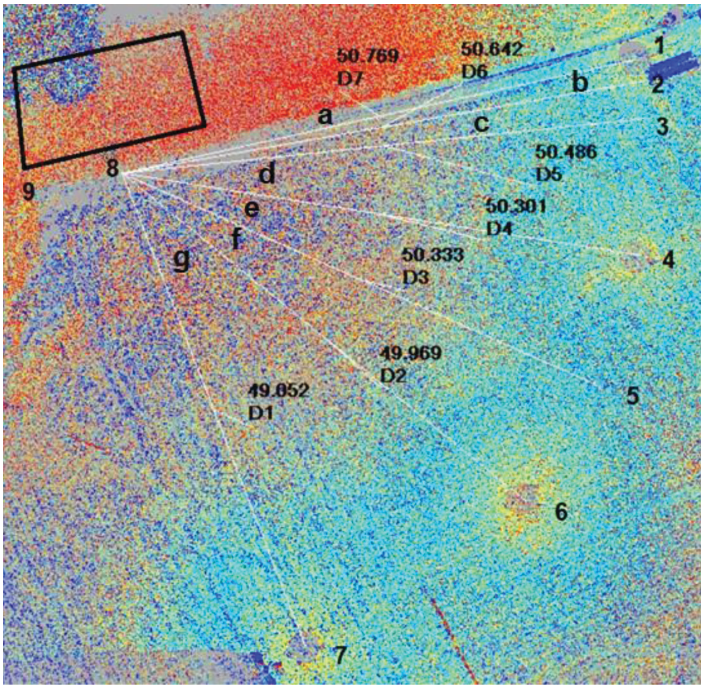

Figure 16: Scanning locations for investigation of effects of incident angle.

Figure 16 represents the sloping surface that was scanned from scanner locations 1 to 7 which resulted in different incident angles. A small patch of the scanned surface near '8' was taken, and DTMs generated for all scan locations. Base DTM was taken from location '7' because of the least incident angle among seven scanning locations, and DTMs resulting from scan locations other than '7' were subtracted from it to see the incident angle effects.

Figure 16 has been generated from the original point cloud using ScanMaster software from scanning stations 1, 4, 6 and 7. Point cloud from scanning locations 2, 3 and 5 are not displayed to make occluded areas of other scanning locations visible in the figure. The main theme behind this experimental setup was to scan the target area from a location to have the maximum possible incident angle and at the same time to keep other sources of error as minimum as possible. All scanning locations from 1 to 7 were manually measured using measuring tape from location '8', which is almost in the centre of the bottom line of the rectangular scanned location, to remove any error due to range difference. All distances from scanning stations to location '8' are measured and annotated using ScanMaster software. It can be seen that the range difference is approximately within 1.5 m distance which is so small that it will result in an equal contribution of error due to range, if any, in final products, which will be eliminated during DTM differences.

Angles between lines joining scanner locations '1' to '7' to location '8' are marked as alphabets from 'a' to 'g' and are also measured using ScanMaster software and are as shown in Table 3.

Table 2: Incident angles relative to scanned locations.

Angle ID as in Figure 16	Average Incident Angle with Rectangular Patch centre line (deg)
a	86.3
b	83.4
c	79.4
d	64.3
e	49.2
f	34.1
g	3.4

The narrow scanning angles coupled with the slope of rectangular location results in average incident angles ranging from approximately 4^0 to 87^0. In order to reduce the error due to resolution, all scanning was carried out using a high resolution of 6.3 mm at10 m.

7.2 Data Acquisition and Processing

To minimize the errors due to registration/georeferencing, all scan locations were referred to the position at location '9', which is slightly on one side of the rectangular patch. The scanner was initially placed at location '9', and coordinates of all scanning locations were measured using prisms at scanning locations relative to arbitrary coordinates of location '9'. Subsequently, the scanner was replaced with a prism at location '9', which acted as backsight for all scanning locations. After data collection, all scans were registered to location '9' using the technique of foresight backsight registration through ScanMaster software. The quality of registration was checked from 'back sight error' and 'occupation errors', which were below mm level.

The small rectangular portion, as mentioned in Figure 16, was cropped from all scans, and new clouds were created. All DTMs were generated using the topo to raster tool of ArcMap, which uses iterative finite difference interpolation technique, an optimized version of local interpolation methods like inverse distance weighted, etc. This is designed for the creation of hydrologically correct DEMs and is based on the ANUDEM program developed by (Hutchinson et al., 2011). The reason for choosing this technique is that it interpolates elevation values for a raster under such constraints, ensuring an output of connected drainage structures and the correct representation of break lines. The constraint of drainage enforcement attempts to remove all sinks or depressions because these are generally errors, since sinks are rare in natural landscapes. A sample DTM from location '7' is as shown in Figure 17.

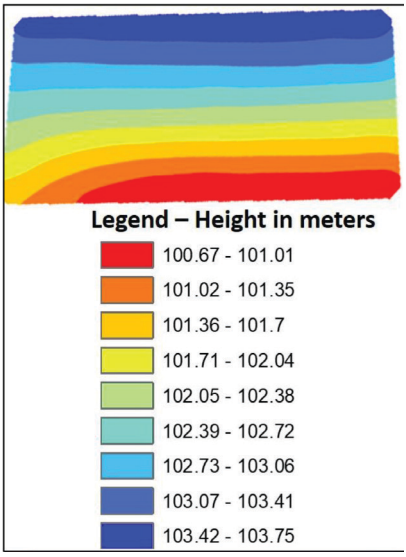

Figure 17: DTM of a small rectangular segment from location 7.

7.3 Results and Analysis

Before creating the DTMs from cropped rectangular area point clouds of all seven locations, the number of points of all cropped scans was noted one by one from ScanMaster software (Table 4).

Table 3: Number of points from different scan locations.

Scanning Location	Number of Points of cropped Scan	Average Incident Angle with Rectangular Patch centre line (deg)
1	7759	86.3
2	10560	83.4
3	13972	79.4
4	24710	64.3
5	31958	49.2
6	37991	34.1
7	41946	3.4

It can be seen that as the scan angle decreases, i.e. incident angle increases, the number of points decreases. The decreasing pattern of individual points with respect to the increase in incident angle is as shown in Figure 18.

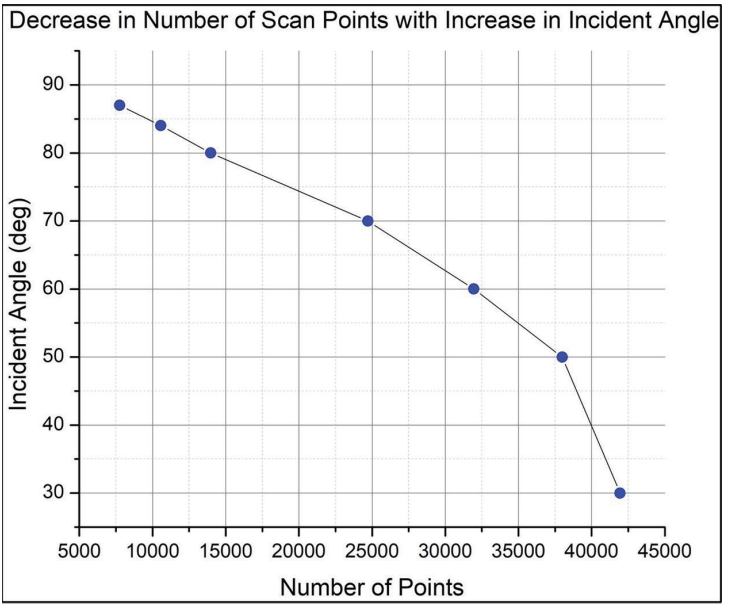

Figure 18: Variation of the number of scan points with change in incident angle.

It can be noted from Figure 18 that the incident angle and the corresponding number of scan points are inversely proportional and are also almost linearly related to each other. The regression analysis rendered the value of Multiple R as 0.964, which means that both incident angle and number of points are strongly linearly correlated. The decrease in the number of points with an increase in incident angle depends on the surface roughness. Smooth surfaces will lose more points as compared to rough surfaces. It can be explained in any of the following ways:

a. There may be no return signal at a large incident angle and smooth surface at all due to a large reflection angle.
b. There may be less energy reflected back and detected as the noise at a large incident angle and rough surface because of lower intensity than a threshold.
c. In the case of a rougher surface, reflected energy might be re-reflected in another direction due to the masking effect.

To quantify the error contribution due to incident angle, seven DTMs were created. The DTM of scanning location number '7' was used as the base DTM because of the least incident angle. All other six DTMs were subtracted using the raster algebra tool of ArcMap (Table 5).

Column 2 of Table 5 depicts the mean difference between DTMs which can be termed the mean error because it can be presumed that DTM generated from scanning location having minimum incident angle will be the most accurate. In this case, DTM from location '7' has the least incident angle. This is because all other error sources contribute in the same amount that cancels during difference except

the incident angle effect. It can also be noted from column 2 of Table 5 that the mean difference values become negative, which means that with an increase in incident angle, the error in the height of DTM also increases (Figure 19).

Table 4: Mean error and standard deviation in DTM differences.

DTM Difference	Mean Error (m)	Standard Deviation (σ) (m)
Loc 7 – Loc 6	0.0069	0.0095
Loc 7 – Loc 5	-0.0119	0.0043
Loc 7 – Loc 4	-0.0023	0.0095
Loc 7 – Loc 3	-0.0070	0.0119
Loc 7 – Loc 2	-0.0134	0.0102
Loc 7 – Loc 1	-0.0257	0.0146

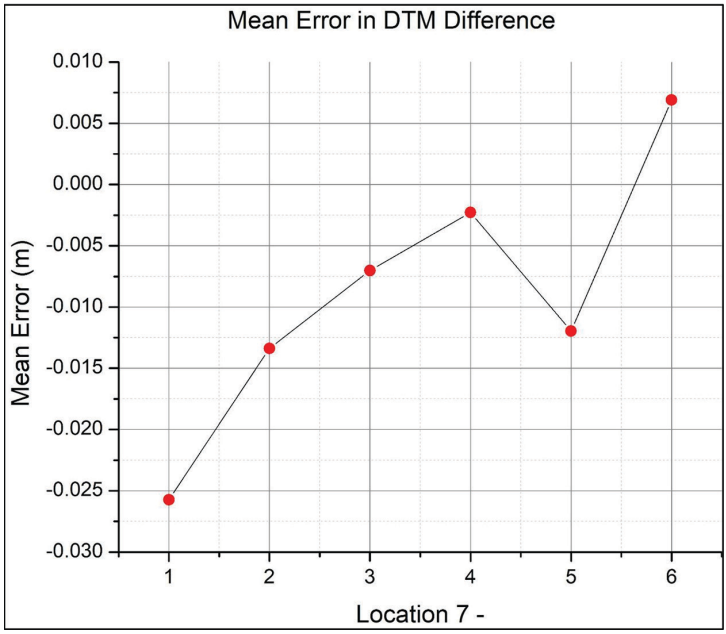

Figure 19: Variation in mean difference (error) among DTMs scanned from different incident angles.

Figure 19 depicts that the error in DTMs increases as the incident angle increases, and both are strongly related linearly if DTM of location 5 is considered as an outlier. If location 5 is not considered an outlier, then the regression analysis renders the value of Multiple R as 0.834 and is considered an outlier than 0.973. In both cases, however, incident angle and error can be considered linearly related.

8 CONCLUSION

Terrestrial laser scanners are widely used in fulfilling diverse type of surveying needs. This paper presented a scan planning approach to minimize the effects of incident angle and laser beam footprint size on both error budget and LOD. This approach has been realized using sensor models that relate different

scan geometry parameters and helps in scanner placement, which ensures required LOD and precision beforehand, leading to optimized scan planning considering the effects of laser beam incident angle and footprint size. The mathematical models have been developed for different surface configurations and verified mathematically by deriving one model from other surface models by changing the parameters. The combined error budget due to incident angle and laser footprint size has been studied on the natural landscape inside the UTM campus.

These models can be used beforehand as guiding principles for positioning the TLS in such a way to ensure accurate data collection at user-specified LOD, which will result in an economic approach ensuring completeness, reduced data and collection time and less processing time. It is recommended that these models may be incorporated in the next generations of TLS so as to get optimized data instead of redundant data due to fear of incompleteness.

Literature and references:

Abdullah, C. C. K., Baharuddin, N., Ariff, M., Majid, Z., Lau, C., Yusoff, A., Idris, K., Aspuri, A. (2017). Integration of Point Clouds Dataset from Different Sensors. The International Archives of Photogrammetry, Remote Sensing and Spatial Information Sciences, XLII-2/W3. DOI: https://doi.org/10.5194/isprs-archives-xlii-2-w3-9-2017

Bruce, D., Crosby, C., Carr, S. (2016). TLS Field Methods Manual. https://d32ogoqmya1dw8.cloudfront.net/files/.../tls_field_methods_manual.v2.pdf, accessed 5. 7. 2019.

Cheng, L., Chen, S., Liu, X., Xu, H., Wu, Y., Li, M., Chen, Y. (2018). Registration of laser scanning point clouds: A review. Sensors, 18 (5), 1641. DOI: https://doi.org/10.3390/s18051641

Daliga, K., urałowicz, Z. (2016). Examination method of the effect of the incidence angle of laser beam on distance measurement accuracy to surfaces with different colour and roughness. Boletim de Ciências Geodésicas, 22 (3), 420–436. DOI: https://doi.org/10.1590/s1982-21702016000300024

Hutchinson, M. F., Xu, T., Stein, J. A. (2011). Recent progress in the ANUDEM elevation gridding procedure. Geomorphometry, 2011, 19–22. https://gisandscience.com/2011/12/15/recent-progress-in-the-anudem-elevevation-gridding-procedure, accessed 3. 5. 2019.

Kaasalainen, S., Jaakkola, A., Kaasalainen, M., Krooks, A., Kukko, A. (2011). Analysis of incidence angle and distance effects on terrestrial laser scanner intensity: Search for correction methods. Remote Sensing, 3 (10), 2207–2221. DOI: https://doi.org/10.3390/rs3102207

Kandrot, S. M. (2013). Coastal Monitoring: A New Approach. Chimera. http://research.ucc.ie/journals/chimera/2013/00/kandrot/09/en, accessed 15. 11. 2019.

Kersten, T. P., Mechelke, K., Lindstaedt, M., Sternberg, H. (2008). Geometric Accuracy Investigations of the Latest Terrestrial Laser Scanning Systems. Paper presented at the Integrating Generations FIG Working Week 2008, Stockholm, Sweden. www.fig.net/pub/fig2008/papers/ts02d/ts02d_01_%20mechelke_etal_2785.pdf, accessed on 11. 2. 2019.

Kersten, T. P., Mechelke, K., Lindstaedt, M., Sternberg, H. (2009). Methods for geometric accuracy investigations of terrestrial laser scanning systems. Photogrammetrie-Fernerkundung-Geoinformation, 2009 (4), 301–315. DOI: https://doi.org/10.1127/1432-8364/2009/0023

Kościuk, J. (2012). Modern 3D scanning in modelling, documentation and conservation of architectural heritage. Wiadomości Konserwatorskie, 82–88. http://yadda.icm.edu.pl/yadda/element/bwmeta1.element.baztech-article-BPK6-0025-0071, accessed 21. 3. 2019.

Lichti, D., Franke, J., Cannell, W., Wheeler, K. (2005b). The potential of terrestrial laser scanners for digital ground surveys. Journal of Spatial Science, 50 (1), 75–89. DOI: https://doi.org/10.1080/14498596.2005.9635039

Lichti, D. D. (2007). Error modelling, calibration and analysis of an AM–CW terrestrial laser scanner system. ISPRS Journal of Photogrammetry and Remote Sensing, 61 (5), 307–324. DOI: https://doi.org/10.1016/j.isprsjprs.2006.10.004

Lichti, D. D. (2010a). A review of geometric models and self-calibration methods for terrestrial laser scanners. Boletim de Ciências Geodésicas, 16 (1). https://revistas.ufpr.br/bcg/article/view/17242, accessed 18. 2. 2020.

Lichti, D. D., Gordon, S. J., Tipdecho, T. (2005a). Error models and propagation in directly georeferenced terrestrial laser scanner networks. Journal of Surveying Engineering, 131 (4), 135–142. DOI: https://doi.org/10.1061/(asce)0733-9453(2005)131:4(135)

Luh, L. C., Setan, H., Majid, Z., Chong, A. K., an, Z. (2014). High resolution survey for topographic surveying. Paper presented at the IOP Conference Series: Earth and Environmental Science. DOI: https://doi.org/10.1088/1755-1315/18/1/012067

Mahmood, S., Majid, Z., Idris, K. M. (2020). Terrestrial LiDAR sensor modeling towards optimal scan location and spatial density planning for 3D surveying. Applied Geomatics. DOI: https://doi.org/10.1007/s12518-020-00320-9

Mahmood, S., Majid, Z., Idris, K. M., Zainuddin, K. (2018). Geometric and Radiometric Characteristics of Terrestrial Laser Scanning-A Review. International Journal of Pure and Applied Mathematics, 118 (24). https://acadpubl.eu/hub/2018-118-24/1/43.pdf, accessed 10. 12. 2019.

Pinkerton, M. (2011). Terrestrial laser scanning for mainstream land surveying. Survey Quarterly, 300 (65), 7. https://www.fig.net/resources/proceedings/fig_proceedings/fig2010/papers/fs03d/fs03d_pinkerton_3814.pdf, accessed 20. 10. 2018.

Reshetyuk, Y. (2009). Self-calibration and direct georeferencing in terrestrial laser scanning. Doctoral Dissertation, KTH. https://www.diva-portal.org/smash/record.jsf?pid=diva2%3A139761&dswid=452, accessed 21. 3. 2017.

Russhakim, N. A. S., Ariff, M. F. M., Majid, Z., Idris, K. M., Darwin, N., Abbas, M. A., Zainuddin, K., Yusoff, A. R. (2019). The suitability of terrestrial laser scanning for building survey and mapping applications. The International Archives of the Photogrammetry, Remote Sensing and Spatial Information Sciences, XLII-2/W9. DOI: https://doi.org/10.5194/isprs-archives-XLII-2-W9-663-2019

Schaer, P., Skaloud, J., Landtwing, S., Legat, K. (2007). Accuracy estimation for laser point cloud including scanning geometry. Paper presented at the Mobile Mapping Symposium 2007, Padova. https://infoscience.epfl.ch/record/116146, accessed 18. 6. 2017.

Sheng, Y. (2008). Quantifying the size of a lidar footprint: A set of generalized equations. IEEE Geoscience and Remote Sensing Letters, 5 (3), 419–422. DOI: https://doi.org/10.1109/lgrs.2008.916978

Soudarissanane, Lindenbergh, Gorte, B. (2008). Reducing the error in terrestrial laser scanning by optimizing the measurement set-up. Proceedings of International Archives of Photogrammetry, Remote Sensing and Spatial Information Sciences, 3–11. https://www.researchgate.net/publication/229037307, accessed 10. 11. 2019.

Soudarissanane, Lindenbergh, R., Menenti, M., Teunissen, P. (2011). Scanning geometry: Influencing factor on the quality of terrestrial laser scanning points. ISPRS Journal of Photogrammetry and Remote Sensing, 66 (4), 389–399. DOI:https://doi.org/10.1016/j.isprsjprs.2011.01.005

Soudarissanane, S. (2016). The geometry of terrestrial laser scanning; identification of errors, modeling and mitigation of scanning geometry. TU Delft, Delft University of Technology. https://repository.tudelft.nl/islandora/object/uuid:b7ae0bd3-23b8-4a8a-9b7d-5e494ebb54e5, accessed 20. 6. 2019.

Soudarissanane, S., Lindenbergh, R., Menenti, M., Teunissen, P. (2009). Incidence angle influence on the quality of terrestrial laser scanning points. Paper presented at the Proceedings ISPRS Workshop Laserscanning 2009, 1-2 Sept 2009, Paris, France. https://gnss.curtin.edu.au/wp-content/uploads/sites/21/2016/04/Soudarissanane2009Incidence.pdf, accessed 25. 9. 2019.

Tan, K., Cheng, X. (2016). Correction of incidence angle and distance effects on TLS intensity data based on reference targets. Remote Sensing, 8 (3), 251. DOI: https://doi.org/10.3390/rs8030251

Topcon. (2019). Topcon Positioning Systems, Inc. https://www.topconpositioning.com/mass-data-and-volume-collection/laser-scanners/gls-2000 accessed on 06-05-2019

Voegtle, T., Wakaluk, S. (2009). Effects on the measurements of the terrestrial laser scanner HDS 6000 (Leica) caused by different object materials. Proceedings of ISPRS Work, 38, 68–74. https://www.isprs.org/proceedings/xxxviii/3-W8/papers/68_laserscanning09.pdf, accessed 15. 10. 2017.

Zámečníková, M., Neuner, H., Pegritz, S., Sonnleitner, R. (2015). Investigation on the influence of the incidence angle on the reflectorless distance measurement of a terrestrial laser scanner. Vermessung & Geoinformation, 2 (3).

Mahmood S., bin Majid Z., bin M. Idris K., Hamid Chaudhry M. (2021). Influence of incident angle and laser footprint on precision and level of detail in terrestrial laser scanner measurements. Geodetski vestnik, 65 (2), 260-281.
DOI: https://doi.org/10.15292/geodetski-vestnik.2021.02.260-281

Corresponding author: Assist. Prof. Dr . Sajid Mahmood
National University of Sciences and Technology (NUST), College of Civil Engineering
Campus Risalpur 24080, Pakistan
e-mail: smehmood@mce.nust.edu

Dr. Khairulnizam bin M. Idris
University Technology Malaysia, Faculty of Built Environment and Surveying
81310 Johor Bahru, Malaysia
e-mail: khairulnizami@utm.my

Assoc. Prof. Dr. Zulkepli bin Majid
University Technology Malaysia, Faculty of Built Environment and Surveying
81310 Johor Bahru, Malaysia
e-mail: zulkeplimajid@utm.my

Assist. Prof. Muhammad Hamid Chaudhry
GIS Center at the University of the Punjab Lahore, Pakistan
e-mail: hamid.gis@pu.edu.pk